FORSCHUNGSZENTRUM
ROSSENDORF e.V.

FZR

FZR-71
February 1995
Preprint

B. Heide and H.W. Barz

Collective Effects and Multifragmentation in Heavy Ion Collisions at Intermediate Energies within a Hybrid Model

Forschungszentrum Rossendorf e.V.
Postfach 51 01 19 · D-01314 Dresden
Bundesrepublik Deutschland

Telefon (0351) 591 3263
Telefax (0351) 591 3700
E-Mail heide@fz-rossendorf.de
barz@fz-rossendorf.de

Collective Effects and Multifragmentation in Heavy Ion Collisions at Intermediate Energies within a Hybrid Model

B. HEIDE[a,b] AND H. W. BARZ[b,a]

[a] *Institut für Kern- und Hadronenphysik, FZ Rossendorf, Pf 510119, 01314 Dresden, Germany*
[b] *Institut für Theoretische Physik, Technische Universität Dresden, Mommsen Str. 13, 01062 Dresden, Germany*

Abstract:
Central and semi-central Au + Au collisions at 150 A·MeV and 250 A·MeV are investigated in the framework of a hybrid model with dynamical and statistical components. Starting from the BUU approach an ansatz for the Wigner function is made which describes thermal and collective motion of the nucleons and models the transition from the one-source to the two-source behaviour. Anisotropic flow energies and temperatures as well as angular momentum are extracted. Nucleonic flow and pre-equilibrium emission reduce considerably the excitation energy of the matter. The cluster formation is described by the Copenhagen multifragmentation model. Charge spectra, energy spectra and two-particle correlations of the fragments are reproduced. Agreement with experiment can be improved by assuming a reduced transverse flow.

1 Introduction

Heavy-ion collisions offer the possibility to study extremely heated and compressed nuclear matter. The break-up process of such a matter is called multifragmentation. It leads to many intermediate mass fragments (IMFs) which are defined here as fragments with charge ≥ 3. Very sophisticated detectors have been developed in order to measure IMFs. The experiments (see e. g. [1]) initiated many theoretical studies. Although it is generally assumed that multifragmentation is connected with a liquid-vapour phase transition (c. f. [2, 3, 4, 5]) the final proof is lacking and multifragmentation is still not fully understood.

In nearly central heavy ion collisions at energies of several hundreds of MeV a very short lived hot region is formed. On the first view it seems to be unlikely that, at this large energies, a source is formed which decays in many IMFs. If the energy would be equally distributed among the degrees of freedom an immediate vaporization would take place. At the same time very large radial flow was established which contains roughly one third of the available center-of-mass energy [6, 7]. The presence of nucleonic flow was predicted long time ago [8] and is the backbone of the application of hydrodynamics to heavy ion collisions. This large collective motion reduces considerably the energy which can be distributed randomly over the remaining degrees of freedom and which is available for statistical fragmentation of the nuclei. In addition, non-equilibrium emission of light fragments is also essential. This is well known from measurements of source sizes which always turn out to be smaller than one would expect from the nucleon number of the total system [9].

From the theoretical point of view the violent phase and the fragmentation phase should be treated with the same dynamical model. At present such a model is not at hand although much progress has been achieved recently. Molecular dynamical models (see e. g. [10, 11]) are most promising which can take into account many-body correlations on a classical basis trying to include quantum mechanical aspects by representing each nucleon by a wave packet. The present molecular-dynamical transport models are quite successful in describing collective effects (e. g. bounce-off, squeeze-out). They fail, however, in reproducing the observed fragment multiplicities [12, 13, 14]. An extension of these molecular-dynamical descriptions is provided by the fermionic molecular-dynamical model [15]. In this model the Pauli-principle is regarded by an antisymmetrized product of wave packets and the widths of the wave packets are dynamical parameters. The equations of motion are derived from a quantum variational principle. However, the large computational effort needed has prevented an application of this model to nuclei with mass numbers above 40 until now.

Alternatively to such models, one can construct so-called hybrid models [16, 17, 18] on the basis of the Boltzmann-type transport equation. These models make use of the fact that one-particle observables are well described by calculating the one-particle phase-space density[19]. Therefore these models are applied to

describe the evolution of a nucleus-nucleus system from the initial stage of the collision up to the moment at which it breaks into fragments. The final evolution of the system is described by a statistical model. These models [20, 21, 22] are based on the assumption of statistical equilibrium and take into account the quantum states of the formed fragments. They are quite successful in reproducing the observed charge distributions [12, 13, 23].

In order to gain insight into the mechanism of Au on Au collisions at 150 A·MeV and 250 A·MeV incident energy, we have constructed such a hybrid model which consists of the Boltzmann-Uehling-Uhlenbeck model [24] (dynamical model) and the Copenhagen model [22] (statistical model). Special attention will be drawn to the role of the nucleonic flow. In a former work [18] we have analysed the behaviour of the flow pattern as a function of the impact parameter and found a radially symmetric flow for impact parameters smaller than $2.5fm$. For larger impact parameters the flow becomes very asymmetric and the system begins to form two independent fragmenting sources. One aim is to implement this behaviour in the statistical fragmentation model. In this way we are able to treat central collisions on the same footing as semi-central collisions.

Within this hybrid model we shall analyse the two-particle correlation functions as well as the charge and the kinetic energy spectra. Special attention will be drawn to the role of the nucleonic flow and the characteristics of the fragmenting matter (i. e. mass number, volume, excitation energy, temperature and angular momentum).

The paper is organized as follows: At first we give some introductory remarks on the applied Boltzmann-Uehling-Uhlenbeck (BUU) model in section 2 and afterwards on the Copenhagen model in section 3. In the subsequent section we describe in detail how we connect these two models. Then we will discuss the results in section 5 and a summary will be given at the end.

2 The BUU model

The BUU equation [25, 26] describes the time evolution of the single-particle phase-space distribution function f and reads as follows

$$\begin{aligned}
&\tfrac{\partial}{\partial t} f(\vec{r},\vec{p},t) + \tfrac{1}{m_N}\vec{p}\cdot\vec{\nabla}_r f(\vec{r},\vec{p},t) - \vec{\nabla}_r U(r)\cdot\vec{\nabla}_p f(\vec{r},\vec{p},t) = \\
&\quad \tfrac{4\pi}{(2\pi\hbar)^6\hbar}\int d^3p_1' d^3p_2 d^3p_2'\,\delta(\tfrac{1}{2m_N}[p^2+p_2^2-p_1'^2-p_2'^2])\,\delta^3(\vec{p}+\vec{p}_2-\vec{p}_1'-\vec{p}_2')\mid T\mid^2 \\
&\quad \times\{f(\vec{r},\vec{p}_1',t)f(\vec{r},\vec{p}_2',t)[1-f(\vec{r},\vec{p},t)][1-f(\vec{r},\vec{p}_2,t)] \\
&\quad -f(\vec{r},\vec{p},t)f(\vec{r},\vec{p}_2,t)[1-f(\vec{r},\vec{p}_1',t)][1-f(\vec{r},\vec{p}_2',t)]\} \qquad (1)
\end{aligned}$$

Here, T denotes the transition matrix for the transition from the momentum states $\vec{p}_1', \vec{p}_2'$ to states $\vec{p}, \vec{p}_2$ which are influenced by the medium. The integral of $\mid T \mid^2$ over the final momenta $\vec{p}_1'$ and $\vec{p}_2'$ including the two delta functions is

proportional to the in-medium nucleon-nucleon cross section. There are several hints from theoretical [27, 28] as well as from experimental investigations (see e.g. [29]) that the in-medium cross sections might be changed compared to the free ones. However, since this is still an open question we use the free nucleon-nucleon cross section which gives a quite satisfactory agreement concerning the stopping of the nucleons.

For the potential energy per nucleon V and the corresponding mean-field potential U

$$U = \frac{\partial}{\partial n}(n\,V(n)) = c_1\left(\frac{n}{n_0}\right) + c_2\left(\frac{n}{n_0}\right)^{\sigma}, \tag{2}$$

three different parameter sets derived from density-dependent Skyrme forces are taken into account. The parameters $c_1 = -356$ MeV, $c_2 = 303$ MeV, $\sigma = 7/6$ correspond to an incompressibility of $K = 210$ MeV (soft equation of state (EOS)), $c_1 = -218$ MeV, $c_2 = 164$ MeV, $\sigma = 4/3$ refer to $K = 235$ MeV (medium EOS) and $c_1 = -124$ MeV, $c_2 = 70.5$ MeV, $\sigma = 2$ belong to $K = 380$ MeV (stiff EOS). The nuclear matter saturation density n_0 is taken to be 0.168 fm^{-3}.

Eq. (1) is solved using the parallel ensemble method [24, 30]. In our calculations we use 200 test particles per nucleon, a cell size of 1 fm^3 to calculate the density in the coordinate space, and a cell size of $(2\pi\hbar)^3$ is taken to determine the phase-space density used to calculate the collision term on the r.h.s. of eq. (1).

The parallel ensemble method ensures that the mean field (2) has a smooth behaviour and that two-body and higher correlations are washed out. So the algorithm governs the time evolution of the single-particle phase-space density $f(\vec{r},\vec{p},t)$ and describes the expansion of dense and excited matter formed during the collision. Due to the lack of higher correlations it cannot describe the formation of fragments. Further, we remark that although the BUU algorithm is based on a nonrelativistic mean field potential the nucleons obey relativistic kinematics.

To check how well the BUU model describes the experiment of collisions of gold on gold we calculate the transverse momentum which is carried by the nucleons. In the experiment this transverse motion is characterized by the quantity E_{rat} which is defined as ratio of the of transversal to longitudinal kinetic energies seen in the forward hemisphere in the c.m. frame (c. f. Ref. [31])

$$E_{rat} = \left.\frac{\sum_i^N p_{\perp,i}^2/m_N}{\sum_i^N p_{\parallel,i}^2/m_N}\right|_{p_\parallel>0}. \tag{3}$$

We have calculated the E_{rat} distribution and the polar-angle distribution for gold on gold collisions at 150 A·MeV incident energy, see fig. 1 and fig. 2. The E_{rat} distribution was generated for the hard as well as for the soft EOS in the full range

of impact parameters up to $b = 15fm$ (the generation of the E_{rat} distribution by dint of the BUU code is described in appendix A). In fig. 3 we depict the relation between E_{rat} values and the impact parameter assuming a perfect detection of all particles. This relation is used to determine the impact parameters of single events in experiment. Due to the statistical fluctuations an exact mapping is not possible. Detector cuts and trigger conditions make the situation worse.

It is seen in fig. 1, that the BUU calculations agree fairly well with the data for $0.4 < E_{rat} < 1.2$. The peak between $0.2 < E_{rat} < 0.4$ corresponds to large impact parameters. The lack of cross section at small E_{rat} might be due to the fact that the BUU code is not able to produce clusters which certainly become important for large impact parameters. For central and semi-central collisions our BUU model predicts sufficient stopping compared with experiment. Since the stopping depends essentially on the nucleon-nucleon cross section the agreement of E_{rat} with experiment confirms our choice of the cross section.

Fig. 2 shows the polar-angle distribution which is also sensitive to the tranverse flow. One sees clearly that the transverse peaking of the cross section occurs only for very small impact parameters and already disappears for an impact parameter of $1.0fm$. This is in line with our finding in ref. [18]. Due to the limited detector acceptance a straight comparison with experimental values is not possible at present (c. f. [32]).

As one can see from fig. 1 and fig. 3 there is no big difference between the soft and hard EOS. So, we apply the medium one in the remainder of this paper.

3 The statistical multifragmentation model

The fragment formation is described within the framework of the Copenhagen model [22]. The fundamental assumption of the model is that a thermodynamical equilibrium is reached as the matter enters the instable region of nuclear matter. The model is based on Boltzmann's principle:

$$S_f \propto \ln W_f, \tag{4}$$

where S_f denotes the entropy and W_f the statistical weight of state f. The state f can be any final state of the excited system. It is essential that a sufficiently large sample of partitions with fixed nucleon number and excitation energy E^* is taken. The entropy of each configuration is calculated making use of standard thermodynamics. For this purpose a temperature T is associated to each partition by the requirement

$$E^* = \sum_{A,Z} N_{A,Z} \left(E^{int}_{A,Z} + \tfrac{3}{2} T \right), \tag{5}$$

where $N_{A,Z}$ denotes the numbers of the fragments with mass number A and charge number Z. The first part on the r.h.s. is the sum over the internal energies while

the second part is the translational energy per nucleon in the classical limit. The internal energies are determined by means of a liquid-drop model which is generalized to finite temperatures. Since the excitation energy of the system is a given quantity the temperature depends on the actual partition and is a fluctuating quantity.

Now the entropy is calculated for each partition by

$$S_f \equiv S(\{N_{A,Z}\}, T, V_b) = -\sum_{A,Z} N_{A,Z} \left(\frac{\partial}{\partial T} \left[F^T_{A,Z} + F^{int}_{A,Z} \right]_{V_b} \right), \qquad (6)$$

where $F^T_{A,Z}$ is the translational and $F^{int}_{A,Z}$ the internal contribution to the free energy of the fragment.

The statistical multifragmentation model now provides us an ensemble of partitions which are chosen randomly by Monte-Carlo methods with weights according to Boltzmann's principle. The fragments within this partition are highly excited and one has to consider their cooling which is caused by evaporation of light and heavier particles. The evaporation processes are computed on the basis of Weisskopf's statistical compound evaporation model [34]. If a fragment c decays into channel x by emission of a light particle with mass number a_x then the decay rate per kinetic energy E_{kin} is given [35] by

$$\frac{\mathrm{d}^2 N_x}{\mathrm{d}E_{kin}\mathrm{d}t} = \frac{g_x a_x m_N}{\pi^2 \hbar^3} E_{kin}\, \sigma^c_{a+A}\, \mathrm{e}^{S^{int}(A_x, T_x) - S^{int}(A_c, T_c)}, \qquad (7)$$

where g_x is the spin degeneracy factor and A_x, A_c denote the mass number of the residual and initial fragment, respectively. The temperature T_x can be calculated from the initial temperature T_c. For the decay into channel x the rate depends on the compound-nucleus formation cross section $\sigma^c_{a+A} = \pi(R_A + R_a)^2(1 - V_B/E_{kin})\Theta(E_{kin} - V_B)$ with V_B being the Coulomb threshold and Θ standing for the step function.

The life time τ of the fragment is given by integrating the rate function (7) over E_{kin} as $\tau = (\sum_x dN_x/dt)^{-1}$. Assuming an exponential decay law the consecutive decays of a hot fragment are sampled using a Monte-Carlo method. Eq. (7) controls also the energy distribution of the emitted particles. This is important when the kinetic energies of the final cold fragments has to be calculated.

4 The hybrid model

Our hybrid model couples the two models introduced in the foregoing sections. From the BUU calculations we extract the properties of the source, namely nucleon number, break-up volume and excitation energy per nucleon. These quantities determine the break-up in fragments. Further, we extract the velocity distribution of the nucleons and take their collective motion explicitly into account. This velocity distribution will be transferred to the fragments.

It is important to determine the break-up time at which such a transition is to be made. In the highly diluted parts of the matter, nucleons are too far away from each other to form clusters. Therefore we assume that clusters are formed in the internal zone where the density is larger than a certain limiting density n_{limit}. This concept excludes the fast pre-equilibrium particles. These particles take away a large part of the energy of the system. Therefore, the excitation energy of the remaining matter becomes smaller than one expects if the beam energy is equally shared among all nucleons. The limiting density together with the break-up time determines, for a given excitation energy, the number of the fragments which are formed. This is the main criterion which will be used in the following. It has turned out that both parameter are not independent from each other, so small break-up densities are connected to early break-up times.

To extract the collective properties of the velocity pattern we choose a coordinate system given by the principal axes of the energy flow tensor Θ

$$\Theta_{ij} \equiv \frac{1}{2m_N N} \sum_{n=1}^{N} p_i^{(n)} p_j^{(n)}, \tag{8}$$

where the sum runs over all N nucleons with $p_i^{(n)}$ being the i-th component of the nucleon momentum $\vec{p}^{(n)}$ in the c.m. frame of the fragmenting matter, and m_N denotes the nucleon mass. This coordinate system is referred to as Θ-frame. Further we introduce an L-frame which is oriented according the nucleon distribution of the system:

$$L_{ij} \equiv \frac{1}{N} \sum_{n=1}^{N} r_i^{(n)} r_j^{(n)}. \tag{9}$$

At small reaction times the principal axes of this system deviates considerably from the Θ-system.

Now we determine the fragment velocity distribution in two steps. First we make an ansatz for a single-nucleon phase-space density $w(\vec{r}, \vec{p})$. For this purpose we divide the coordinate space into two half-spaces separated by a plane $r_3 = 0$ which is perpendicularly to the largest axis of the ellipsoid of the tensor $\mathbf{L}$ (c. f. left panel of fig. 4). We write for the distribution function $w^>$ in the upper half of the system:

$$w^>(\vec{r}, \vec{p}) \propto f(\vec{r}) \; \mathrm{e}^{-\frac{1}{2}\sum_{i=1}^{3} \Lambda_i (p_i - B_i(r_i - R_i^>) - g_i^>)^2} \tag{10}$$

and a corresponding ansatz $w^<$ for the lower half with vectors $\vec{R}^< = -\vec{R}^>$ and $g_3^< = -g_3^>$. This ansatz is motivated by the position and momentum density picture generated by the BUU approach. A typical picture for an impact parameter of 6 fm at a time of 70 fm/c (related to the moment where the two nuclei touch

each other) is shown in fig. 4. It is seen that there are almost two separated sources for semi-central collisions. The vectors $\vec{R}^<, \vec{R}^>$ and $\vec{g}^<, \vec{g}^>$ denote the centres-of-gravity and the mean momenta in the region above or below the plane, respectively. The quantities B_i as part of the diagonal tensor B characterize an anisotropic radial flow centred around $\vec{R}$. For large impact parameters there is a gap in the velocity distribution at the plane $r_3 = 0$ of the Θ-frame, describing two receding sources. Eq. (10) is also suitable for head-on collisions. In this case the gap disappears and $B_3 * R_3 = g_3$ holds. Then, the distribution functions of the upper and the lower plane merge to a smooth function for a single expanding source with an asymmetric momentum distribution.

The parameters Λ_i give the widths of the distributions around the collective velocity and can be connected to temperatures T_i

$$T_i \;=\; \frac{1}{m_N \Lambda_i} \qquad (i = 1,2,3). \tag{11}$$

For simplicity we assume that the spatial distribution $f(\vec{r}) = 1$ if $\vec{r}$ lies within a cylinder of height $2h$ and radius ϱ and $f(\vec{r}) = 0$ otherwise. The cylinder is parallel to the 3-axis of the L-system. The elements B_i are connected with the expanding flow energies per nucleon $E_{exp.\,flow,i}$ in transverse direction

$$E_{exp.\,flow,i} \;=\; \langle \frac{p_i^2}{2m_N} \rangle = \frac{B_i^2 \varrho^2}{8 m_N} \qquad (i = 1,2), \tag{12}$$

and the flow in longitudinal direction is composed of an expansion and a translational part in the direction of the momentum g_3:

$$E_{flow,3} \;=\; \langle \frac{p_3^2}{2m_N} \rangle = \frac{B_3^2 h^2}{24 m_N} + \frac{g_3^2}{2m_N}. \tag{13}$$

The background of the derivation of eqs. (12) and (13) is provided in B. The parameters h, $\vec{R}$, ϱ, $\vec{g}$, B_i and Λ_i are given in appendix C.

In a similar manner we calculate the rotational motion in the reaction plane. The angular momentum $\vec{J}$ is given by $\vec{J} = \sum_n^N \vec{r}^{(n)} \times \vec{p}^{(n)}$ and the rotational energy $E_{rot} = \frac{1}{2} \vec{J}^{\dagger} \mathrm{M}^{-1} \vec{J}$ with the tensor of inertia $\mathrm{M} = m_N \sum_n (\vec{r}^{(n)\,2} - \mathrm{L})$.

In the second step we transform ansatz (10) into a fragment velocity distribution. In the spirit of the coalescence model one can find this distribution by calculating the overlap of the product of all single-nucleon phase-space densities with the Wigner function W_{frag} of a fragment with mass number A.

$$w^>_{frag}(\vec{r}_{frag}, \vec{v}_{frag}) \;\propto\; \int d^{3A}r\, d^{3A}v \left[\prod_{n=1}^{A} w^>(\vec{r}^{(n)}, \vec{p}^{(n)}) \right] \delta^3\Big(\sum_{n=1}^{A} \vec{r}^{(n)} - A\vec{r}_{frag}\Big) \times$$
$$\delta^3\Big(\sum_{n=1}^{A} \vec{v}^{(n)} - A\vec{v}_{frag}\Big) W_{frag}(\vec{r}^{(n)}, \vec{v}^{(n)}). \tag{14}$$

The two δ-functions define the centre-of-gravity $\vec{r}_{frag}$ and the velocity $\vec{v}_{frag}$ of the fragment.

The coalescence model neglects correlations which evolve during the fragmentation process. This leads generally to an underestimations of the formation probability of fragments with large nucleon number. We use eq. (14) to obtain a guide for the velocity distribution of the fragments by approximating W_{frag} as

$$W_{frag} \quad \propto \quad \prod_{n=2}^{A} \delta^3(\vec{r}^{(1)} - \vec{r}^{(n)}). \tag{15}$$

This means that all nucleons are located at the centre-of-gravity of the fragment. After some algebra we get for respective $w^<$ and $w^>$:

$$w_{frag}(\vec{r}_{frag}, \vec{v}_{frag}) \propto \quad \mathrm{e}^{-\frac{Am_N^2}{2}\sum_{i=1}^{3}\Lambda_i(v_{frag,i} - \frac{B_i}{m_N}(r_{frag,i} - R_i) - \frac{g_i}{m_N})^2}. \tag{16}$$

Hence, the velocity of the fragment is distributed around a flow velocity which is given by $(\mathbf{B}(\vec{r}_{frag} - \vec{R}) + \vec{g})/m_N$. Thus, the fragment obtains a flow energy in proportion to its mass number A while the random part of the motion has a kinetic energy of $\sum T_i/2$ independently of its mass number.

Now, we calculate the excitation energy per nucleon by adding the potential energy $V(n)$ of eq. (2), the average kinetic energy $E_{kin} = \sum_{n=1}^{N} \vec{p}_n^{\,2}/(2m_N N)$ and the Coulomb energy per nucleon $E_{coul} = \sum_{m<n}^{Z} \frac{e^2}{|\vec{r}_n - \vec{r}_m|}/N$ (Z = proton number, e = elementary charge) and subtract the ground state energy per nucleon E_0, the rotational energy E_{rot}, as well as the flow energies:

$$E^* \quad = \quad V(n) + E_{coul} + E_{kin} - E_0 - E_{rot} - \sum_{i=1}^{2} E_{exp.flow,i} - E_{flow,3}. \tag{17}$$

Now, we discuss briefly the relations of our quantities $\vec{g}$ and $\mathbf{B}$ to standard observables for the collective behaviour of nuclear matter. The sidewards flow, observed in non-central collisions, is a complicated function of our parameters. Its value $< p_x >$ at projectile rapidity is roughly given by $g_3 \sin\alpha$, where α denotes the flow angle between the beam axis and the largest principal axis of the energy flow tensor. The slope of the side flow $\frac{d}{dy} < p_x >$ as a function of rapidity y is mainly determined by the ratio $m_N B_1/B_3$. Eq. (16) contains also the effect that the reduced side flow $\frac{d}{dy} < p_x/p_\perp >$ increases with the mass number of the fragment [36]. This is caused by the fact that the flow pattern becomes more elongated with increasing fragment mass due to the translational motion g_3. The squeeze-out phenomenon is connected with the transverse part of the radial flow. It is observed in non-central collisions by the ratio of particles emitted out of the reaction plane and those emitted in the plane. Recent theoretical investigations [37] have shown that this squeeze-out ratio increases with the mass of IMFs. This

of impact parameters up to $b = 15fm$ (the generation of the E_{rat} distribution by dint of the BUU code is described in appendix A). In fig. 3 we depict the relation between E_{rat} values and the impact parameter assuming a perfect detection of all particles. This relation is used to determine the impact parameters of single events in experiment. Due to the statistical fluctuations an exact mapping is not possible. Detector cuts and trigger conditions make the situation worse.

It is seen in fig. 1, that the BUU calculations agree fairly well with the data for $0.4 < E_{rat} < 1.2$. The peak between $0.2 < E_{rat} < 0.4$ corresponds to large impact parameters. The lack of cross section at small E_{rat} might be due to the fact that the BUU code is not able to produce clusters which certainly become important for large impact parameters. For central and semi-central collisions our BUU model predicts sufficient stopping compared with experiment. Since the stopping depends essentially on the nucleon-nucleon cross section the agreement of E_{rat} with experiment confirms our choice of the cross section.

Fig. 2 shows the polar-angle distribution which is also sensitive to the tranverse flow. One sees clearly that the transverse peaking of the cross section occurs only for very small impact parameters and already disappears for an impact parameter of $1.0fm$. This is in line with our finding in ref. [18]. Due to the limited detector acceptance a straight comparison with experimental values is not possible at present (c. f. [32]).

As one can see from fig. 1 and fig. 3 there is no big difference between the soft and hard EOS. So, we apply the medium one in the remainder of this paper.

3 The statistical multifragmentation model

The fragment formation is described within the framework of the Copenhagen model [22]. The fundamental assumption of the model is that a thermodynamical equilibrium is reached as the matter enters the instable region of nuclear matter. The model is based on Boltzmann's principle:

$$S_f \propto \ln W_f, \tag{4}$$

where S_f denotes the entropy and W_f the statistical weight of state f. The state f can be any final state of the excited system. It is essential that a sufficiently large sample of partitions with fixed nucleon number and excitation energy E^* is taken. The entropy of each configuration is calculated making use of standard thermodynamics. For this purpose a temperature T is associated to each partition by the requirement

$$E^* = \sum_{A,Z} N_{A,Z} \left(E^{int}_{A,Z} + \tfrac{3}{2} T \right), \tag{5}$$

where $N_{A,Z}$ denotes the numbers of the fragments with mass number A and charge number Z. The first part on the r.h.s. is the sum over the internal energies while

the second part is the translational energy per nucleon in the classical limit. The internal energies are determined by means of a liquid-drop model which is generalized to finite temperatures. Since the excitation energy of the system is a given quantity the temperature depends on the actual partition and is a fluctuating quantity.

Now the entropy is calculated for each partition by

$$S_f \equiv S(\{N_{A,Z}\}, T, V_b) = -\sum_{A,Z} N_{A,Z} \left(\frac{\partial}{\partial T} \left[F^T_{A,Z} + F^{int}_{A,Z} \right]_{V_b} \right), \qquad (6)$$

where $F^T_{A,Z}$ is the translational and $F^{int}_{A,Z}$ the internal contribution to the free energy of the fragment.

The statistical multifragmentation model now provides us an ensemble of partitions which are chosen randomly by Monte-Carlo methods with weights according to Boltzmann's principle. The fragments within this partition are highly excited and one has to consider their cooling which is caused by evaporation of light and heavier particles. The evaporation processes are computed on the basis of Weisskopf's statistical compound evaporation model [34]. If a fragment c decays into channel x by emission of a light particle with mass number a_x then the decay rate per kinetic energy E_{kin} is given [35] by

$$\frac{\mathrm{d}^2 N_x}{\mathrm{d}E_{kin}\mathrm{d}t} = \frac{g_x a_x m_N}{\pi^2 \hbar^3} E_{kin}\, \sigma^c_{a+A}\, \mathrm{e}^{S^{int}(A_x, T_x) - S^{int}(A_c, T_c)}, \qquad (7)$$

where g_x is the spin degeneracy factor and A_x, A_c denote the mass number of the residual and initial fragment, respectively. The temperature T_x can be calculated from the initial temperature T_c. For the decay into channel x the rate depends on the compound-nucleus formation cross section $\sigma^c_{a+A} = \pi(R_A + R_a)^2(1 - V_B/E_{kin})\Theta(E_{kin} - V_B)$ with V_B being the Coulomb threshold and Θ standing for the step function.

The life time τ of the fragment is given by integrating the rate function (7) over E_{kin} as $\tau = (\sum_x dN_x/dt)^{-1}$. Assuming an exponential decay law the consecutive decays of a hot fragment are sampled using a Monte-Carlo method. Eq. (7) controls also the energy distribution of the emitted particles. This is important when the kinetic energies of the final cold fragments has to be calculated.

4 The hybrid model

Our hybrid model couples the two models introduced in the foregoing sections. From the BUU calculations we extract the properties of the source, namely nucleon number, break-up volume and excitation energy per nucleon. These quantities determine the break-up in fragments. Further, we extract the velocity distribution of the nucleons and take their collective motion explicitly into account. This velocity distribution will be transferred to the fragments.

It is important to determine the break-up time at which such a transition is to be made. In the highly diluted parts of the matter, nucleons are too far away from each other to form clusters. Therefore we assume that clusters are formed in the internal zone where the density is larger than a certain limiting density n_{limit}. This concept excludes the fast pre-equilibrium particles. These particles take away a large part of the energy of the system. Therefore, the excitation energy of the remaining matter becomes smaller than one expects if the beam energy is equally shared among all nucleons. The limiting density together with the break-up time determines, for a given excitation energy, the number of the fragments which are formed. This is the main criterion which will be used in the following. It has turned out that both parameter are not independent from each other, so small break-up densities are connected to early break-up times.

To extract the collective properties of the velocity pattern we choose a coordinate system given by the principal axes of the energy flow tensor Θ

$$\Theta_{ij} \equiv \frac{1}{2m_N N} \sum_{n=1}^{N} p_i^{(n)} p_j^{(n)}, \tag{8}$$

where the sum runs over all N nucleons with $p_i^{(n)}$ being the i-th component of the nucleon momentum $\vec{p}^{(n)}$ in the c.m. frame of the fragmenting matter, and m_N denotes the nucleon mass. This coordinate system is referred to as Θ-frame. Further we introduce an L-frame which is oriented according the nucleon distribution of the system:

$$L_{ij} \equiv \frac{1}{N} \sum_{n=1}^{N} r_i^{(n)} r_j^{(n)}. \tag{9}$$

At small reaction times the principal axes of this system deviates considerably from the Θ-system.

Now we determine the fragment velocity distribution in two steps. First we make an ansatz for a single-nucleon phase-space density $w(\vec{r}, \vec{p})$. For this purpose we divide the coordinate space into two half-spaces separated by a plane $r_3 = 0$ which is perpendicularly to the largest axis of the ellipsoid of the tensor $\mathbf{L}$ (c. f. left panel of fig. 4). We write for the distribution function $w^>$ in the upper half of the system:

$$w^>(\vec{r}, \vec{p}) \propto f(\vec{r}) \; \mathrm{e}^{-\frac{1}{2}\sum_{i=1}^{3} \Lambda_i (p_i - B_i(r_i - R_i^>) - g_i^>)^2} \tag{10}$$

and a corresponding ansatz $w^<$ for the lower half with vectors $\vec{R}^< = -\vec{R}^>$ and $g_3^< = -g_3^>$. This ansatz is motivated by the position and momentum density picture generated by the BUU approach. A typical picture for an impact parameter of 6 fm at a time of 70 fm/c (related to the moment where the two nuclei touch

each other) is shown in fig. 4. It is seen that there are almost two separated sources for semi-central collisions. The vectors $\vec{R}^<, \vec{R}^>$ and $\vec{g}^<, \vec{g}^>$ denote the centres-of-gravity and the mean momenta in the region above or below the plane, respectively. The quantities B_i as part of the diagonal tensor $\mathbf{B}$ characterize an anisotropic radial flow centred around $\vec{R}$. For large impact parameters there is a gap in the velocity distribution at the plane $r_3 = 0$ of the Θ-frame, describing two receding sources. Eq. (10) is also suitable for head-on collisions. In this case the gap disappears and $B_3 * R_3 = g_3$ holds. Then, the distribution functions of the upper and the lower plane merge to a smooth function for a single expanding source with an asymmetric momentum distribution.

The parameters Λ_i give the widths of the distributions around the collective velocity and can be connected to temperatures T_i

$$T_i \;=\; \frac{1}{m_N \Lambda_i} \qquad (i = 1, 2, 3). \tag{11}$$

For simplicity we assume that the spatial distribution $f(\vec{r}) = 1$ if $\vec{r}$ lies within a cylinder of height $2h$ and radius ϱ and $f(\vec{r}) = 0$ otherwise. The cylinder is parallel to the 3-axis of the L-system. The elements B_i are connected with the expanding flow energies per nucleon $E_{exp.\,flow,i}$ in transverse direction

$$E_{exp.\,flow,i} \;=\; \langle \frac{p_i^2}{2m_N} \rangle = \frac{B_i^2 \varrho^2}{8 m_N} \qquad (i = 1, 2), \tag{12}$$

and the flow in longitudinal direction is composed of an expansion and a translational part in the direction of the momentum g_3:

$$E_{flow,3} \;=\; \langle \frac{p_3^2}{2m_N} \rangle = \frac{B_3^2 h^2}{24 m_N} + \frac{g_3^2}{2m_N}. \tag{13}$$

The background of the derivation of eqs. (12) and (13) is provided in B. The parameters h, $\vec{R}$, ϱ, $\vec{g}$, B_i and Λ_i are given in appendix C.

In a similar manner we calculate the rotational motion in the reaction plane. The angular momentum $\vec{J}$ is given by $\vec{J} = \sum_n^N \vec{r}^{(n)} \times \vec{p}^{(n)}$ and the rotational energy $E_{rot} = \frac{1}{2} \vec{J}^{\dagger} \mathbf{M}^{-1} \vec{J}$ with the tensor of inertia $\mathbf{M} = m_N \sum_n (\vec{r}^{(n)\,2} - \mathbf{L})$.

In the second step we transform ansatz (10) into a fragment velocity distribution. In the spirit of the coalescence model one can find this distribution by calculating the overlap of the product of all single-nucleon phase-space densities with the Wigner function W_{frag} of a fragment with mass number A.

$$w^>_{frag}(\vec{r}_{frag}, \vec{v}_{frag}) \;\propto\; \int d^{3A}r\, d^{3A}v \left[\prod_{n=1}^{A} w^>(\vec{r}^{(n)}, \vec{p}^{(n)}) \right] \delta^3\Big(\sum_{n=1}^{A} \vec{r}^{(n)} - A\vec{r}_{frag}\Big) \times$$
$$\delta^3\Big(\sum_{n=1}^{A} \vec{v}^{(n)} - A\vec{v}_{frag}\Big) W_{frag}(\vec{r}^{(n)}, \vec{v}^{(n)}). \tag{14}$$

The two δ-functions define the centre-of-gravity $\vec{r}_{frag}$ and the velocity $\vec{v}_{frag}$ of the fragment.

The coalescence model neglects correlations which evolve during the fragmentation process. This leads generally to an underestimations of the formation probability of fragments with large nucleon number. We use eq. (14) to obtain a guide for the velocity distribution of the fragments by approximating W_{frag} as

$$W_{frag} \quad \propto \quad \prod_{n=2}^{A} \delta^3(\vec{r}^{(1)} - \vec{r}^{(n)}). \tag{15}$$

This means that all nucleons are located at the centre-of-gravity of the fragment. After some algebra we get for respective $w^<$ and $w^>$:

$$w_{frag}(\vec{r}_{frag}, \vec{v}_{frag}) \propto \quad \mathrm{e}^{-\frac{Am_N^2}{2}\sum_{i=1}^{3}\Lambda_i(v_{frag,i} - \frac{B_i}{m_N}(r_{frag,i} - R_i) - \frac{g_i}{m_N})^2}. \tag{16}$$

Hence, the velocity of the fragment is distributed around a flow velocity which is given by $(\mathbf{B}(\vec{r}_{frag} - \vec{R}) + \vec{g})/m_N$. Thus, the fragment obtains a flow energy in proportion to its mass number A while the random part of the motion has a kinetic energy of $\sum T_i/2$ independently of its mass number.

Now, we calculate the excitation energy per nucleon by adding the potential energy $V(n)$ of eq. (2), the average kinetic energy $E_{kin} = \sum_{n=1}^{N} \vec{p}_n^{\,2}/(2m_N N)$ and the Coulomb energy per nucleon $E_{coul} = \sum_{m<n}^{Z} \frac{e^2}{|\vec{r}_n - \vec{r}_m|}/N$ (Z = proton number, e = elementary charge) and subtract the ground state energy per nucleon E_0, the rotational energy E_{rot}, as well as the flow energies:

$$E^* \quad = \quad V(n) + E_{coul} + E_{kin} - E_0 - E_{rot} - \sum_{i=1}^{2} E_{exp.flow,i} - E_{flow,3}. \tag{17}$$

Now, we discuss briefly the relations of our quantities $\vec{g}$ and $\mathbf{B}$ to standard observables for the collective behaviour of nuclear matter. The sidewards flow, observed in non-central collisions, is a complicated function of our parameters. Its value $< p_x >$ at projectile rapidity is roughly given by $g_3 \sin\alpha$, where α denotes the flow angle between the beam axis and the largest principal axis of the energy flow tensor. The slope of the side flow $\frac{d}{dy} < p_x >$ as a function of rapidity y is mainly determined by the ratio $m_N B_1/B_3$. Eq. (16) contains also the effect that the reduced side flow $\frac{d}{dy} < p_x/p_\perp >$ increases with the mass number of the fragment [36]. This is caused by the fact that the flow pattern becomes more elongated with increasing fragment mass due to the translational motion g_3. The squeeze-out phenomenon is connected with the transverse part of the radial flow. It is observed in non-central collisions by the ratio of particles emitted out of the reaction plane and those emitted in the plane. Recent theoretical investigations [37] have shown that this squeeze-out ratio increases with the mass of IMFs. This

effect is not contained in eq. (10) which has a symmetric spatial distribution. Fig. 5 shows that the momentum perpendicular to the reaction plane is enhanced for moderate impact parameters.
At last, we have to fix the break-up time $t_{break-up}$. It is chosen such that a reasonable break-up density is reached. A limiting density $n_{limit} = n_0/7$ is used which is compatible with the assumption of the statistical multifragmentation model. The break-up time is taken to be 65 fm/c and 55 fm/c after touching of the nuclei for the reaction of gold on gold at 150 A·MeV and 250 A·MeV, respectively. For larger bombarding energies the system expands faster and the break-up starts earlier.

In fig. 5 we show the volume of the ellipsoid of the energy flow tensor versus time for a beam energy of 150 A·MeV. The volume rises in the compression stage and declines during the expansion. It has nearly reached its minimum value at the chosen break-up times.

Having obtained the properties of the source we can implement them into the statistical multifragmentation model. Every event is created in accordance with the probability (4) and the positions of the fragments are distributed randomly within the cylinder in the L-frame. Then we determine the momenta of the fragments by means of relation (16) in the Θ-frame. Afterwards the positions and the momenta are transformed back in the laboratory frame. The following expansion of the fragments is described by Newtonian equations which take into account only the mutual Coulomb forces between the fragments. During the expansion the hot fragments emit statistically light particles and cool down. The emission rates and the energy distributions are simulated by a Monte-Carlo method based on eq. (7).

As the result of the calculation we obtain finally a statistical ensemble of cold fragments with given velocities taking into account the most important correlations produced by the Coulomb repulsion.

5 Results and discussion

5.1 Properties of the fragmenting matter

Using the break-up times mentioned in the foregoing section we represent in fig. 6 the mass number, the excitation energy and the volume of the fragmenting matter as well as the temperatures as a function of the impact parameter b. Dividing the mass number by the volume one gets break-up densities between $\frac{1}{5}\,n_0$ and $\frac{1}{4}\,n_0$ for collisions at 150 A·MeV beam energy for different impact parameters. For collisions at 250 A·MeV beam energy, break-up densities between $\frac{1}{6}\,n_0$ and $\frac{1}{4}\,n_0$ have been obtained. Similar values were found in refs. [38, 39].

The excitation energy (17) is shown in fig. 6 for both bombarding energies. The maximum values around 12 MeV are obtained for small impact parameters.

Smaller values of about 5 MeV refer to impact parameters around $8fm$. The values are similar for both bombarding energies, however they belong to quite different mass numbers. The excitation energy together with the break-up density influence sensitively the number of IMFs calculated within the statistical multifragmentation model.

The temperature parameters T_i rise with the impact parameter, cf. fig. 6. However, one would expect a higher temperature for head-on collisions than for semi-central collisions. The behaviour shown in fig. 6 is connected with the pure classical ansatz for the distribution function (10) together with eq. (11) which interpretes Fermi motion as temperature. A solution of this problem has been has been proposed in ref.[40] by using Fermi-Dirac distributions for the nucleons a method which requires large numerical expense. In our analysis this problem is of minor importance since the thermal energies are smaller than the bombarding energy in the centre-of mass system and small compared to the flow energies we are interested in.

Now we turn to the flow properties of the source which are shown in fig. 7 for bombarding energies of 150 A·MeV and 250 A·MeV, respectively. For impact parameters $b \leq 4fm$ the translational flow parameter g_3 and the parameter B_3 of the radial expansion describe together a flow in the 3-direction which linearly rises from the origin of the centre-of-mass system, because relation $B_3 * R_3 = g_3$ is fulfilled. Therefore, we have depicted the sum (13) of the corresponding energies in fig. 7. For larger impact parameters the two sources recede from each other, and we plot the translational part separately from the radial part. One recognizes that the transverse flow energy $E_{exp.flow,1}$ and $E_{exp.flow,2}$ smoothly decreases with rising impact parameter. Also the total radial flow energy diminishes for large impact parameter which explains that the ALADIN measurements [41] has found only marginal effects of flow in contrast to central collisions. The energy contained in the translational motion approaches the bombarding energy for large impact parameter. For small impact parameters the flow is nearly spherically symmetric. We mention that for very central collisions ($b \leq 0.5fm$) the particle flux $\mathrm{d}N/\mathrm{d}\cos\theta$ is even sidewards peaked as we have already seen in fig. 2.

Fig. 8 shows the angular momentum of the source. The total angular momentum is mainly given by the input of the incoming projectile and is only meaningful for very central collisions. For impact parameters larger than 4 fm the rotational motion is much smaller if considered locally. The two sources which are created separately get angular momentum due to the mutual friction of the remnants of target and projectile. As can be seen from fig. 8 each half of the fragmenting matter gets a relative small angular momentum. Its maximum value of about 100 $\hbar$ is reached at $b = 5fm$ and the corresponding rotational energy amounts to 0.5 MeV per nucleon only. The rotation of the total system is already included in the ansatz (10) for the phase space distribution by the translational term g_3 together with the twist between the Θ- and the L- system.

To compare our further calculations with experiment we define central events

to have impact parameters values between 0 fm and 3.5 fm and semi-central ones, which include the central events too, to have impact parameters values between 0 fm and 8 fm. This is in accordance with the experimental cuts [6, 42], where central events belong to the PM5 class and semi-central ones to the PM3-PM5 class.

The charge spectra obtained by the statistical multifragmentation model are depicted in fig. 9 for central and semi-central gold on gold collisions. We find a satisfactory agreement for the IMF production. The discrepancy for charge $Z = 1$ might be due to the fact that light fragments as deuterons and tritons may be formed by coalescense of the pre-equilibrium particles which are not considered within the statistical model. The deviation for charges $Z \geq 9$ do not play an important role in our further analysis because these fragments are very rare.

5.2 One-particle kinetic energy spectra

One-particle spectra of IMFs are very sensitive to the amount of flow since, without flow, the fragments obtain only the small amount of thermal energy. In fig. 10 we compare the calculated spectra of lithium, berylium, boron and carbon isotopes for central gold on gold collisions at 150 A·MeV beam energy with experiment. We recognize that the heavier the fragment the better the agreement between theoretical and experimental values is. Obviously the heavier fragments have sufficient flow whereas the lighter have not. This leads to the suggestion that the flow might depend on the projectile mass. This is understandable from eq. (14), but contradicts to eq. (16). Without using the zero-range approximation (15) the formation of heavy fragments needs the integration over a large volume. Therefore, heavy fragments are formed with larger probability in the inner region of the fragmenting source, where they obtain only a small amount of flow energy.

From the spectra one extracts usually the mean kinetic energy as a function of the mass number and obtains the flow energy according to $E_{kin} = \frac{3}{2}T + AE_{flow}$. Using this formula we get a flow energy of 18 MeV for 150 A·MeV in rough agreement with experiment [7]. For 250 A·MeV we get 25 MeV. From the flow values shown in fig. 7 one obtaines respective values of 12 MeV and 19 MeV only. Part of this difference comes from a final Coulomb acceleration which is also proportional to the fragment mass. In addition the kinetic energy increases by the recoil which the fragments obtain by evaporating particles. Further, we mention that the impact parameter selection is very essential since the measurements are made in forward direction between 25 and 45 degrees in the centre-of-mass system. Contributions from larger impact parameters contain also a certain part of translational motion of the projectile remnant.

5.3 Two-particle velocity distributions

A widely used tool [1, 43, 45] for the investigation of final state interactions is the two-particle correlation function C_2 defined as the ratio of the two-particle velocity distribution Y_{12} to the mixed two-particle velocity distribution $Y_{12,mix}$ calculated by mixing two different events:

$$C_2(v_{red}) \equiv \frac{Y_{12}(v_{red})}{Y_{12,mix}(v_{red})}, \tag{18}$$

where v_{red} denotes the reduced relative velocity [46] between two fragments with charge numbers Z_1 and Z_2, $v_{red} \equiv \mid \vec{v_1} - \vec{v_2} \mid /\sqrt{Z_1 + Z_2}$. Both velocity distributions are normalized to the same number of detected pairs.

The correlation function C_2 is translationally invariant and contains valuable information about the dynamics of the fragmenting source (see e. g. [1]). For IMFs it can be calculated by trajectory calculations since quantum mechanical effects are not important because the distance between the fragments is much larger than their wave length. The Coulomb forces between IMFs suppress the correlation function for values smaller than $v_{red} \approx 0.04c/\sqrt{d/fm}$ independently of the fragment charges, where the quantity d is the average inter-fragment distance. Thus, the size of this Coulomb hole measures the break-up density and, henceforth, the source radius. However, C_2 is also sensitive to other variables like flow and secondary evaporation of light particles. Because of this fact the interpretation of the function C_2 is not trivial.

For central collisions we compare the velocity distributions together with the corresponding correlation functions with experiment in fig. 11. The calculations have been performed by reducing $E_{exp.flow,1}$ and $E_{exp.flow,2}$ by a factor of 2. Otherwise they would have peaked at too a large reduced velocity similarly to the results of ref. [18, 47]. The Coulomb hole of the correlation function is only slightly influenced by the radial flow justifying the standard method for the estimation of the break-up density.

Next, we turn to semi-central events. The correlation functions and the corresponding velocity distributions are displayed in fig. 12. For consistency reasons the tranverse flow has been reduced in the same manner as for central collisions. In contrast to the central collisions the correlation function exhibits a clear peak at $v_{red} = 0.02$ c. It originates from the finite flow angle together with the small aspect ratio $\frac{1}{2}(\Theta_{11} + \Theta_{22})/\Theta_{33}$ of the flow tensor. Both effects make the flow pattern very sensitive to the azimuthal angle. Therefore, the mixed velocity distribution $Y_{12,mix}$ is much wider than the true one Y_{12}. The peak disappears if all events are rotated into a unique reaction plane [45].

Although there is an overall agreement with experiment the size of the Coulomb hole of the computed correlation function differs distinctly from the experimental one at 250 A·MeV beam energy for semi-central collisions. We propose two different explanations to improve the agreement. On the one hand

one could reduce the transverse flow further. The crosses in fig. 12 refer to a reduction by a factor of four. However, there is no reason to assume that the nucleonic flow is transferred differently as a function of energy. On the other hand the break-up density could be diminished. For a very small break-up density, however, the statistical multifragmentation models would predict charge spectra which fall off much stronger than observed. This would mean that the fragments are not formed in thermodynamical equilibrium but rather in a non-equilibrium scenario as it is claimed by the QMD models, see e.g. ref. [10].

6 Summary

We have constructed a hybrid model to analyse central and semi-central collisions at 150 A·MeV and 250 A·MeV beam energy. The model consists of both the BUU model and the Copenhagen model. In addition we we have adjusted the nucleonic phase-space distribution by the ansatz of eq. (10) to the results of the BUU calculations. This distribution takes into account the effect that around an impact parameter of $4fm$ the reaction changes its pattern from a one-source to a two-source behaviour. From this ansatz the phase-space distribution (16) for fragments is derived.

Our approach is based on the idea that in the collision centre an equilibrated source is formed which has fewer particles and less energy then the total colliding system. Intermediate mass fragments are formed in this source which is defined as consisting of nuclear matter with a density larger than about 1/7 of normal matter density. This source fragments when the momenta of the nucleons are relaxed and the flow ellipsoid has shrunk nearly to its asymptotic value. Under this conditions we found relatively moderate excitation energies ranging from 12 MeV down to 5 MeV and source sizes between one and two thirds of the total mass number for impact parameters up to 8 fm which are covered by the recent experiments we have analysed. The multifragmentation of these sources leads to charge spectra in agreement with experiment. The effect of angular momentum was found to be unimportant for the calculation of excitation energies.

The BUU calculations reproduce well the experimental E_{rat} distribution of nucleons. It turned out that the polar-angle distribution exhibits a peak at very central collisions and the shape of the flow pattern is spherically symmetric. For impact parameters larger than 4 fm two sources are formed which recede from each other and their excitation energies become remarkably lower. For very central collisions the flow energy was 12 and 19 MeV per nucleon. These values are about 5 MeV smaller than those obtained from the calculated kinetic energy spectra. We have explained this difference by the additional energy gain by Coulomb expansion after break-up and the recoil which the fragments obtain from the evaporation processes during this expansion. The analysis of the one-particle kinetic spectra has revealed that the flow of heavier fragments might be

smaller than that of lighter ones. However, the quality of the agreement is not good enough to allow a quantitative statement.

Finally, we have discussed the two-particle velocity distributions. The peak in the correlation function for semi-central collisions is explained by the finite angle between flow ellipsoid and beam direction and by the small transverse flow compared to the longitudinal flow. As this ratio decreases with increasing bombarding energy the peak increases. The small Coulomb suppression observed at high energies in the correlation function could not be explained satisfactorily and might hint to the fact that at high energies one approaches the limit of the validity of equilibrium models.

Acknowledgements

The authors thank R. Kotte, W. Neubert, W. Reisdorf, D. Wohlfarth, B. Naumann, P. Danielewicz, B. Kämpfer, R. Wünsch and G. Soff for stimulating discussions. B. H. and H. W. B. acknowledge support by the German BMFT (contract 06DR107).

Appendix A

GENERATION OF THE $d\sigma/d(E_{rat})$ DISTRIBUTION.

To calculate the E_{rat} distribution it is essential that fluctuations are taken into account. This is not possible in standard BUU model. To circumvent this problem we have made use of the parallel ensemble method and have identified every ensemble with one event.

In the calculation we have included the filter routine of the plastic wall of the FOPI collaboration [48] together with the rapidity condition $y_{particle} > y_{cm}$ and have used impact parameters up to $15fm$.

Appendix B

SOME ASPECTS OF FLOW.

The flow analysis is based on the assumption that the velocity of the matter increases linearly as a function of the distance from the centre. This is a good approximation to the flow pattern obtained in BUU calculations where the mean velocity is curved only for very large distances. Then, for a spherically symmetric radial flow the momentum of a nucleon at distance $\vec{r}$ reads

$$\vec{p}_{flow} = \alpha\vec{r}, \tag{B.1}$$

where the quantity α can now determined by a least square fit of eq.(B.1) to the nucleon momenta $\vec{p}^{(n)}$:

$$\frac{\partial}{\partial\alpha}\sum_{n=1}^{N}\left(\vec{p}^{(n)} - \alpha\vec{r}^{(n)}\right)^2 = 0. \tag{B.2}$$

This leads to the kinetic energy of a spherical velocity field

$$E_{spherical\,flow} = \frac{\left(\sum_{n=1}^{N}\vec{p}^{(n)}\cdot\vec{r}^{(n)}\right)^2}{2m_N N\sum_{n=1}^{N}\left(\vec{r}^{(n)}\right)^2}. \tag{B.3}$$

This concept is easily extended to asymmetric flow defining three different flow energies corresponding to the main axis k of the Θ-frame:

$$E_{flow,k} = \frac{\left(\sum_{n=1}^{N}p_k^{(n)}r_k^{(n)}\right)^2}{2m_N N\sum_{n=1}^{N}\left(r_k^{(n)}\right)^2} \tag{B.4}$$

which is the basis of eqs. (12), (13) and (C.5).

We mention finally that the following unequality relations hold:

$$\sum_{k=1}^{3} \Theta_{kk} \;\geq\; \sum_{k=1}^{3} E_{flow,k} \;\geq\; E_{spherical\ flow}. \tag{B.5}$$

Appendix C

PARAMETERS OF THE ANSATZ FOR THE SINGLE-NUCLEON PHASE-SPACE DENSITY.

The parameters h, $\vec{R}$, ϱ, $\vec{g}$, B_i and Λ_i read

$$h = \tfrac{2}{O_{33}} \langle r_3 \rangle , \tag{C.1}$$

$$\vec{R} = \tfrac{h}{2} \vec{e}_3 \tag{C.2}$$

$$\varrho = 2 \sqrt{(\langle r_1^2 \rangle - O_{31}^2 \tfrac{h^2}{3})/(1 - O_{31}^2)} , \tag{C.3}$$

$$\vec{g} = \langle p_3 \rangle \vec{e}_3, \tag{C.4}$$

$$B_i = (\langle p_i r_i \rangle - \tfrac{h}{2} O_{33} g_3 \delta_{3i})/(\langle r_i^2 \rangle - (\tfrac{h}{2} O_{3i})^2), \tag{C.5}$$

$$\Lambda_i = (\langle p_i^2 \rangle - B_i \langle p_i r_i \rangle - (g_3 - O_{33} B_3 \tfrac{h}{2}) g_3 \delta_{3i})^{-1}, \tag{C.6}$$

where the average value of a quantity ξ is defined by $\langle \xi \rangle \equiv \int \xi w \, d^3r d^3p$. The matrix elements O_{ij} determine the transformation between Θ- and L-frame and the coordinates p_i and r_i in the equations above are calculated in the Θ-frame.

References

[1] J. Pochodzalla, postdoctorial thesis, GSI report, GSI-91-11, ISSN 0171-4546 and references therein.

[2] P.J. Siemens, Nature 305(1983)410.

[3] A. D. Panagiotou, M. W. Curtin, H. Toki, D. K. Scott, P. J. Siemens, Phys. Rev. Lett. 52 (1984) 496.

[4] C.J. Pethick and D.G. Ravenhall, Ann. Phys.(N.Y.) 183 (1988) 131.

[5] D. H. E. Gross, Nucl. Phys. A553 (1993) 175c.

[6] N. Herrmann, Nucl. Phys. A553(1993)739c.

[7] C.J. Jeong et al. (FOPI collaboration), Phys. Rev. Lett. 72 (1994) 3486.

[8] W. Scheid, H. Müller and W. Greiner, Phys. Rev. Lett. 32 (1974) 741;
M. Sobel, P. Siemens, J. Bondorf and H. Bethe, Nucl. Phys. A251 (1975) 302.

[9] J. Pochodzalla, W. Trautmann, U. Lynen, Phys. Lett. B232 (1889) 41.

[10] J. Aichelin, Phys. Reports 202 (1991) 233.

[11] D. H. Boal and J. N. Glosli, Phys. Rev. C38 (1988) 1870.

[12] D. R. Bowman et al., Phys. Rev. Lett. 67 (1991) 1527.

[13] R. T. de Souza et al., Phys. Lett. B268 (1991) 6.

[14] G. Peilert et al., Phys. Rev. C39 (1989) 1402.

[15] H. Feldmeier, K. Bieler, J. Schnack, GSI preprint, GSI-94-44 (1994), Nucl. Phys. A, in press.

[16] G. Peilert, Ph. D. thesis, GSI report, GSI-92-13, ISSN 0171-4546.

[17] D. R. Bowman et al., Phys. Rev. C46 (1992) 1834.

[18] B. Heide and H. W. Barz, Phys. Lett. B337 (1994) 53 and erratum Phys. Lett. B340 (1994) 267.

[19] H. Stöcker and W. Greiner, Phys. Reports 137 (1986) 277;
G. F. Bertsch and S. Das Gupta, Phys. Reports 160 (1988) 189.

[20] J. Randrup and S. E. Koonin, Nucl. Phys. A356 (1981) 223.

[21] Sa Ban-hao and D.H.E. Gross, Nucl. Phys. A437 (1985) 643; D.H.E. Gross, Zhang Xiao-ze and Xu Shu-yan, Phys. Rev. Lett. 56 (1986) 1544; X.Z. Zhang et al., Nucl. Phys. A641 (1987) 641.

[22] J. P. Bondorf, R. Donangelo, I. N. Mishustin, C. J. Pethik, H. Schulz and K. Sneppen, Nucl. Phys. A443 (1985) 321;
J. P. Bondorf, R. Donangelo, I. N. Mishustin and H. Schulz, Nucl. Phys. A444 (1985) 460;
H. W. Barz, J. P. Bondorf, R. Donangelo, I. N. Mishustin and H. Schulz, Nucl. Phys. A448 (1986) 753.

[23] K. Hagel et al., Phys. Rev. Lett. 68 (1992) 2141.

[24] W. Bauer, G. F. Bertsch, W. Cassing and U. Mosel, Phys. Rev. C34 (1986) 2127;
W. Bauer, Phys. Rev. Lett. 61 (1988) 2534.

[25] W. Cassing, postdoctorial thesis, GSI report, GSI-86-6; W. Cassing, Z. Phys. A326 (1987) 21.

[26] P. Danielewicz, Ann. Phys. (New York) 152 (1984) 239.

[27] A. Bohnet, N. Ohtsuka, J. Aichelin, R. Linden and Amand Faessler, Nucl. Phys. A494 (1989) 349.

[28] W. Cassing, V. Metag, U. Mosel and K. Niita, Phys. Rep. 188 (1990) 363

[29] G. Westfall et al., Phys. Rev. Lett. 71 (1993) 1986

[30] W. Bauer, G. F. Bertsch and S. Das Gupta, Phys. Rev. Letters 58 (1987) 863.

[31] W. Reisdorf, Proc. Int. Workshop XX on Gross Properties of Nuclei and Nuclear Excitations, Edt. H. Feldmeier, Hirschegg, Austria, Jan. 20-25, 1992, p. 38.

[32] U. Sodan, Ph. D. thesis, University of Heidelberg (1994), unpublished.

[33] Th. Wienold, Ph. D. thesis, University of Heidelberg (1993), GSI report, GSI-93-28, ISSN 0171-4546.

[34] V. Weisskopf, Phys. Rev. 52 (1937) 295;
V. Weisskopf and D. H. Ewing, Phys. Rev. 57 (1940) 472.

[35] W.A. Friedman and W.G. Lynch, Phys. Rev. C28 (1983) 16,950.

[36] K.G.R. Doss et al., Phys. Rev. Lett. 59 (1987) 2720.

[37] C. Hartnack, J. Aichelin, H. Stöcker and W. Greiner, Phys. Lett. B336 (1994) 131.

[38] H. W. Barz, W. Bauer, J. P. Bondorf, A. S. Botvina, R. Donangelo, H. Schulz and K. Sneppen, Nucl. Phys. A561 (1993) 466.

[39] B. Kämpfer et al. (FOPI collaboration), Phys. Rev. C48 (1993) R955.

[40] D.T. Khoa, N. Ohtsuka, Amand Faessler, M. A. Matin, S. W. Huang, E. Lehmann and Y. Lofty, Nucl. Phys. A542 (1992) 671.

[41] V. Lindenstruth et al. (FOPI collaboration), GSI-report, GSI-93-54 (1993).

[42] W. Reisdorf, Proc. Int. Workshop XXII on Gross Properties of Nuclei and Nuclear Excitations, Edt. H. Feldmeier, W. Nörenberg, Hirschegg, Austria, Jan. 17-22, 1994, p. 93.

[43] S. Pratt and M. B. Tsang, Phys. Rev. C36 (1987) 2390.

[44] C. Kuhn et al. (FOPI collaboration), Phys. Rev. C48 (1993) 1232.

[45] R. Kotte et al. (FOPI collaboration), FZ Rossendorf preprint, FZR-56 (1994), submitted to Phys. Rev. C.

[46] Y. D. Kim, R. T. deSouza, C. K. Gelbke, W. G. Gong and S. Pratt, Phys. Rev. C45 (1992) 387.

[47] H. W. Barz and B. Heide, Proc. Int. Workshop XXII on Gross Properties of Nuclei and Nuclear Excitations, Edt. H. Feldmeier, W. Nörenberg, Hirschegg, Austria, Jan. 17-22, 1994, p. 93.

[48] Roland Kotte, private communication.

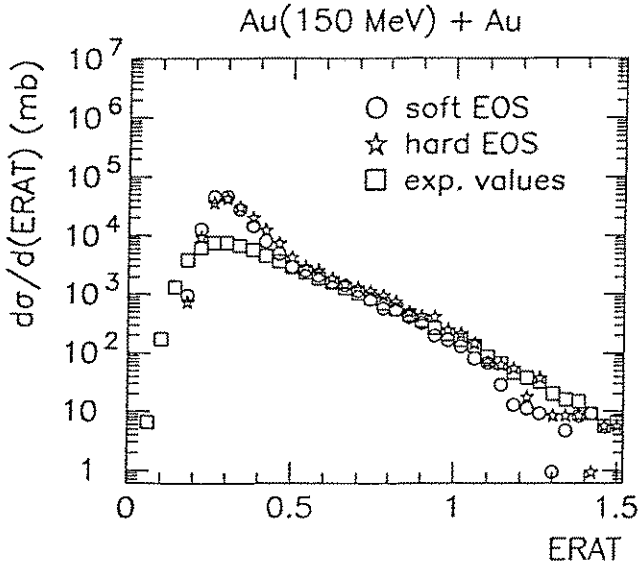

Fig. 1 Calculated E_{rat} distribution for the soft and hard EOS, respectively, in comparison with experiment [33].

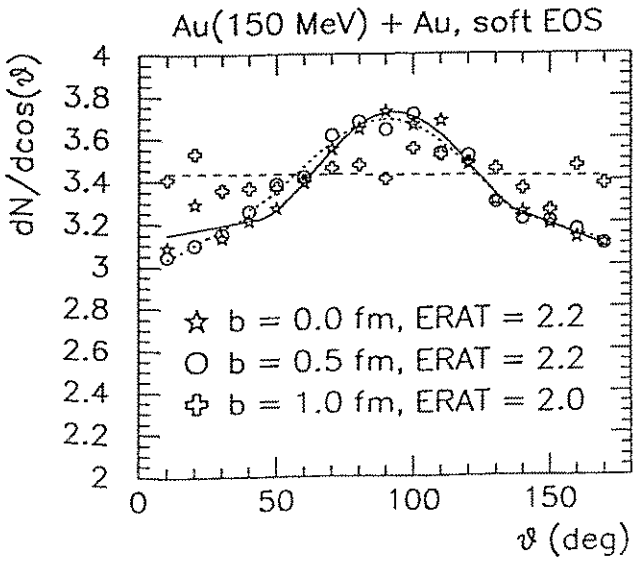

Fig. 2 Polar-angle distribution calculated by use of the soft EOS for three different impact parameters which are equivalent to three different E_{rat} values.

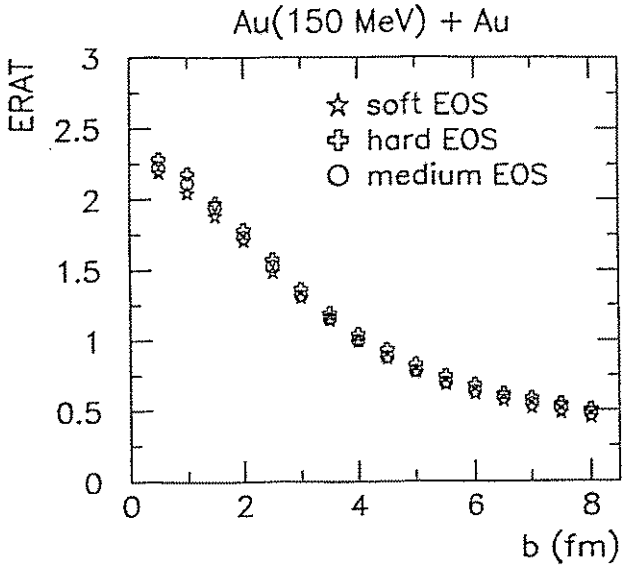

Fig. 3 E_{rat} as a function of the impact parameter b for the soft, medium and hard EOS, respectively. The simulation was done applying a perfect detector.

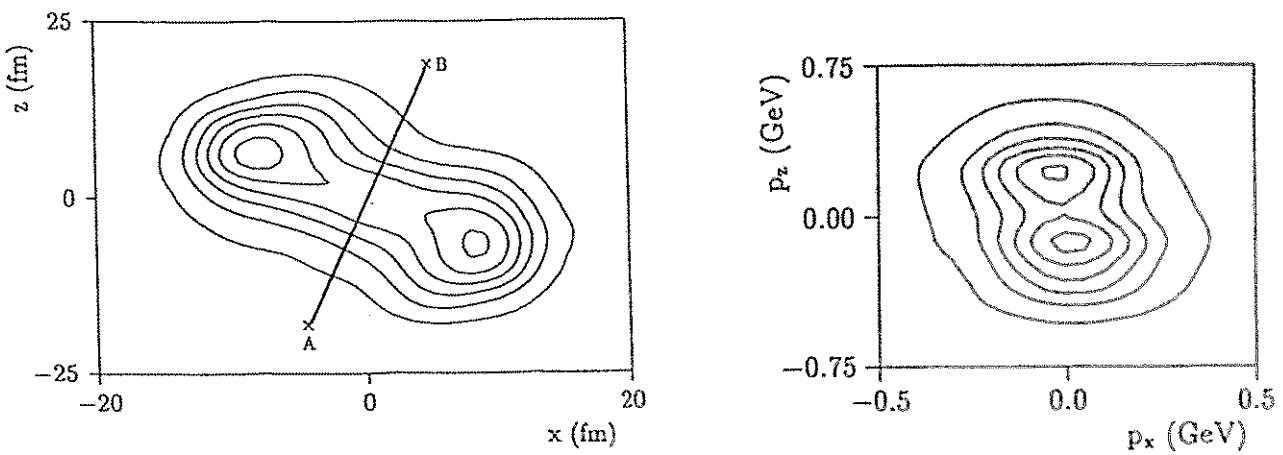

Fig. 4 Position (left) and momentum (right) density distribution for the collision of Au on Au at 150 A·MeV at a time of 70 fm/c. The beam is directed in the z-axis with impact parameter of 6 fm. The points A and B mark the plane which separates the target region from the projectile region. The contour lines are scaled linearly.

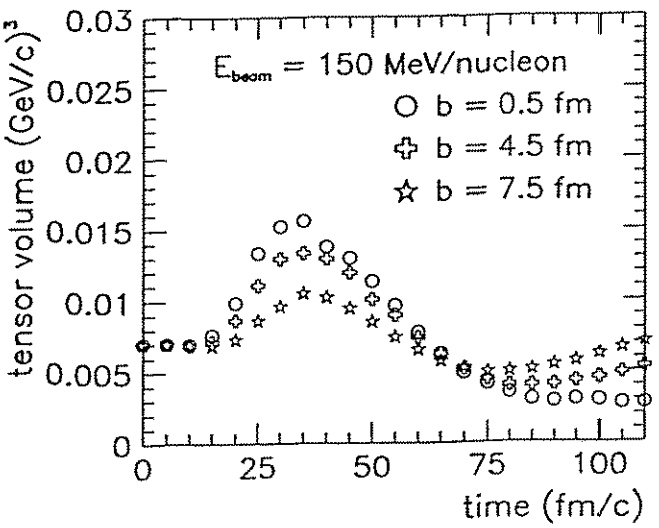

Fig. 5 Volume of the ellipsoid of the energy flow tensor versus the time for several impact parameters. The touching time of the two nuclei is 7 fm/c.

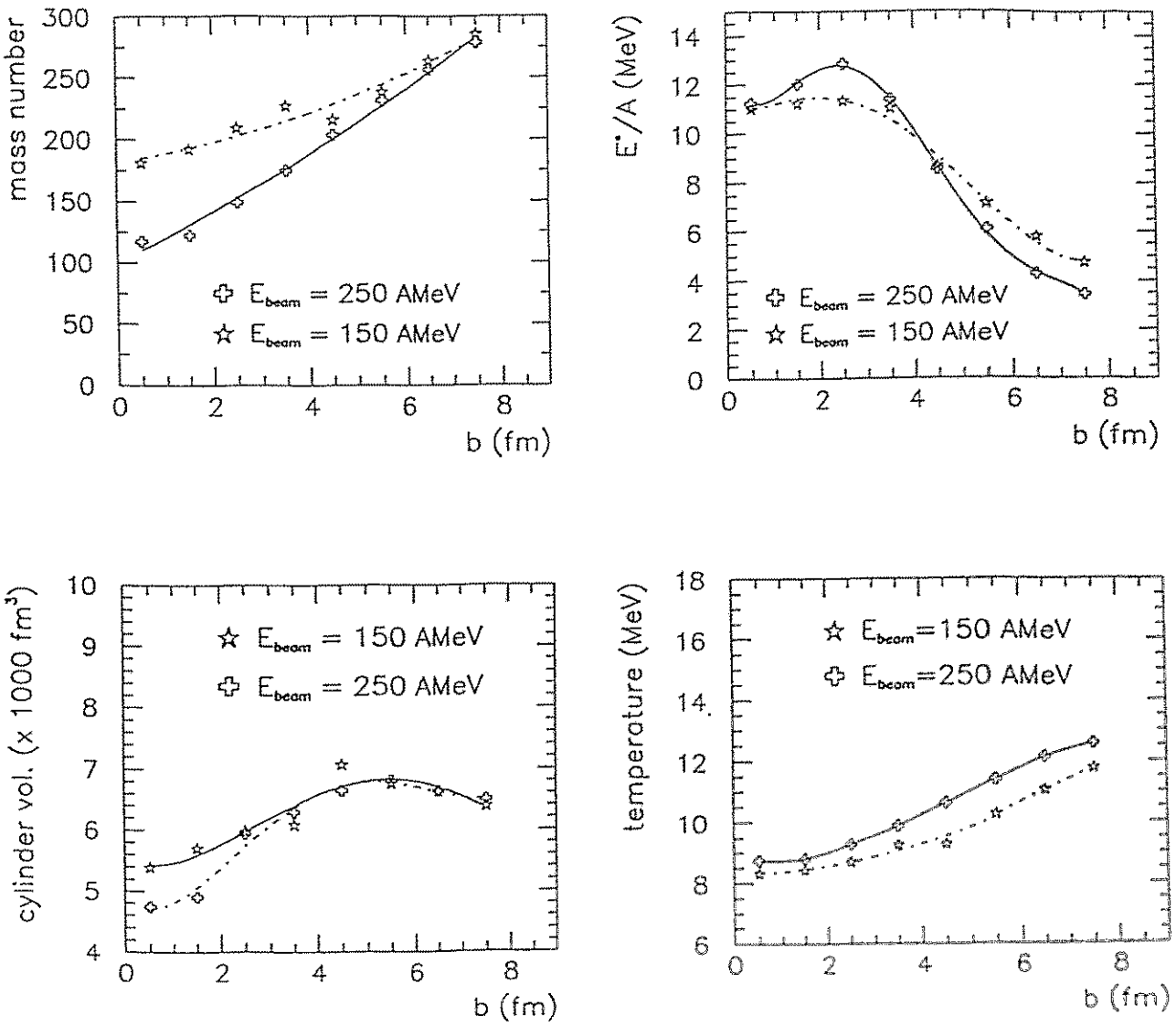

Fig. 6 Mass number, excitation energy, volume and temperature of the fragmenting matter as a function of the impact parameter.

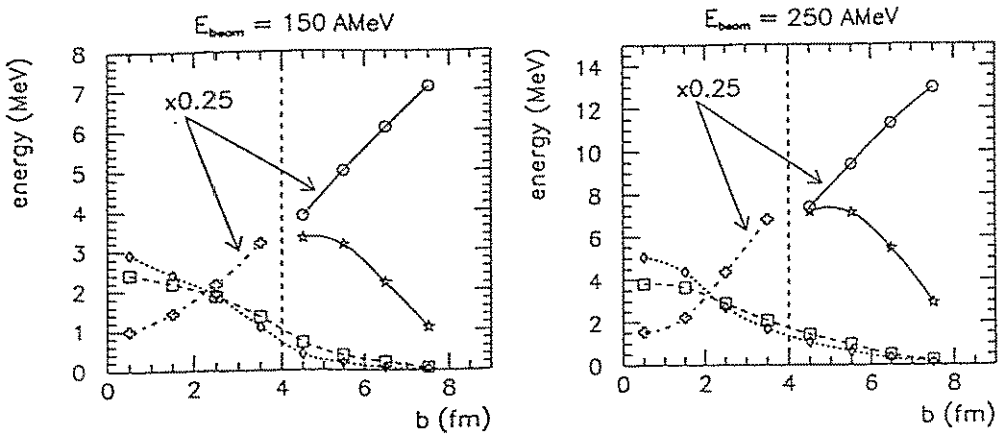

Fig. 7 Flow energies for a beam energy of 150 A·MeV (left panel) and 250 A·MeV (right panel). The flow energy along the flow axis is marked by crosses, in the reaction plane by diamonds and out of plane by squares. For impact parameters larger than 4 fm the energy is split into an translational (circles) and an expanding part (stars) according to eq.(13).

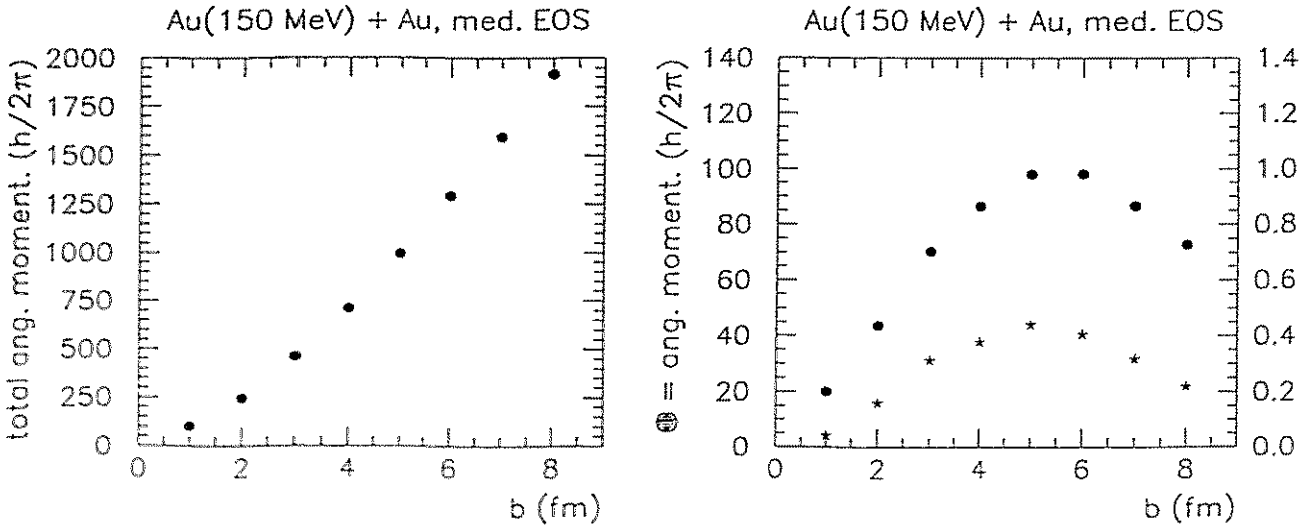

Fig. 8 Angular momenta. The left panel belongs to the total angular momentum of the system. The right panel to one half of the fragmenting matter seen from its own centre-of-gravity. The right scale refers to the kinetic energy of rotation per nucleon.

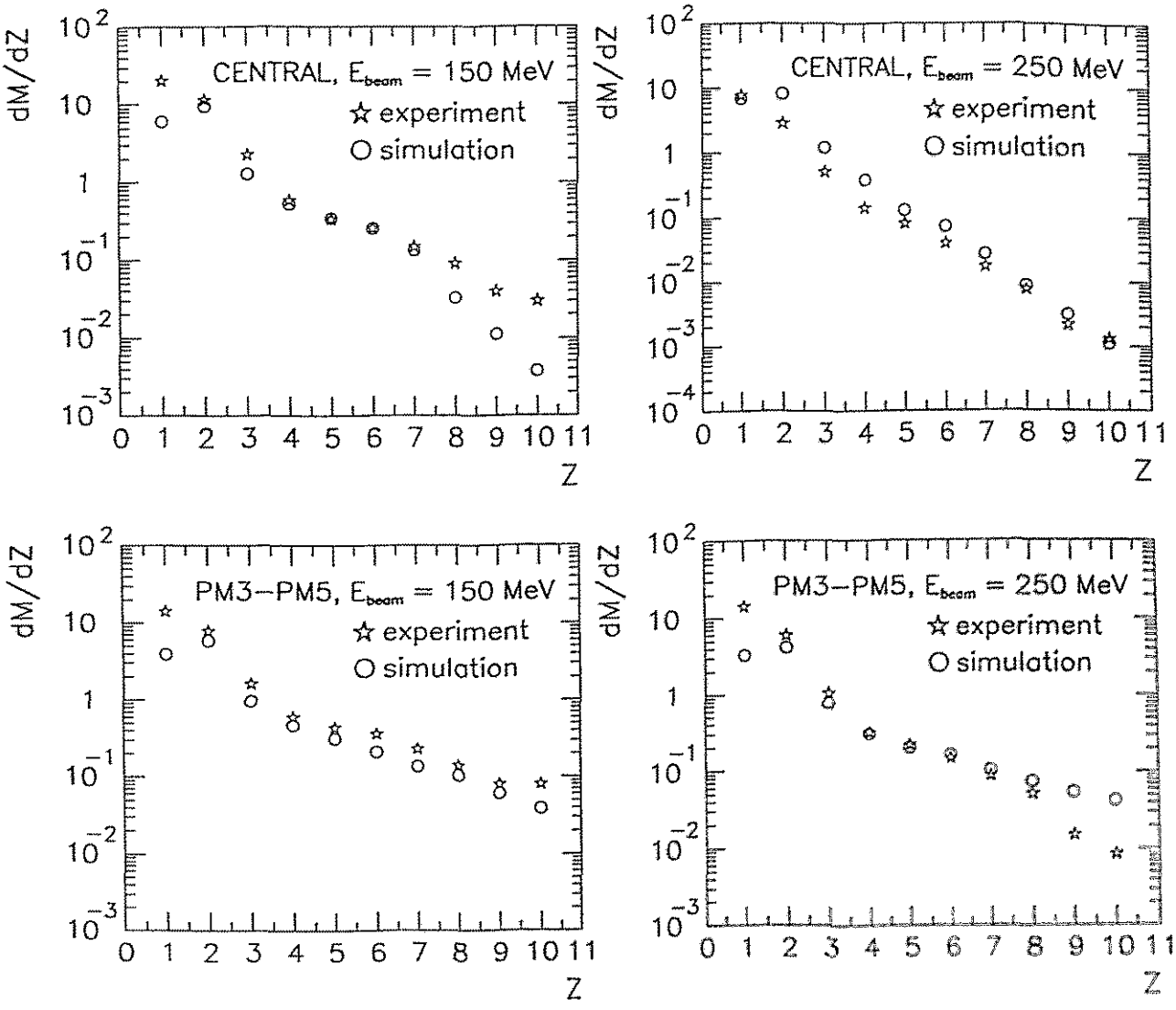

Fig. 9 Charge distributions for central and semi-central gold on gold collisions. The experimental values for central collisions at 150 A·MeV are taken from [44] whereas the ones for semi-central events at 150 A·MeV are gathered from [33]. All experimental data for collisions at 250 A·MeV are taken from [32].

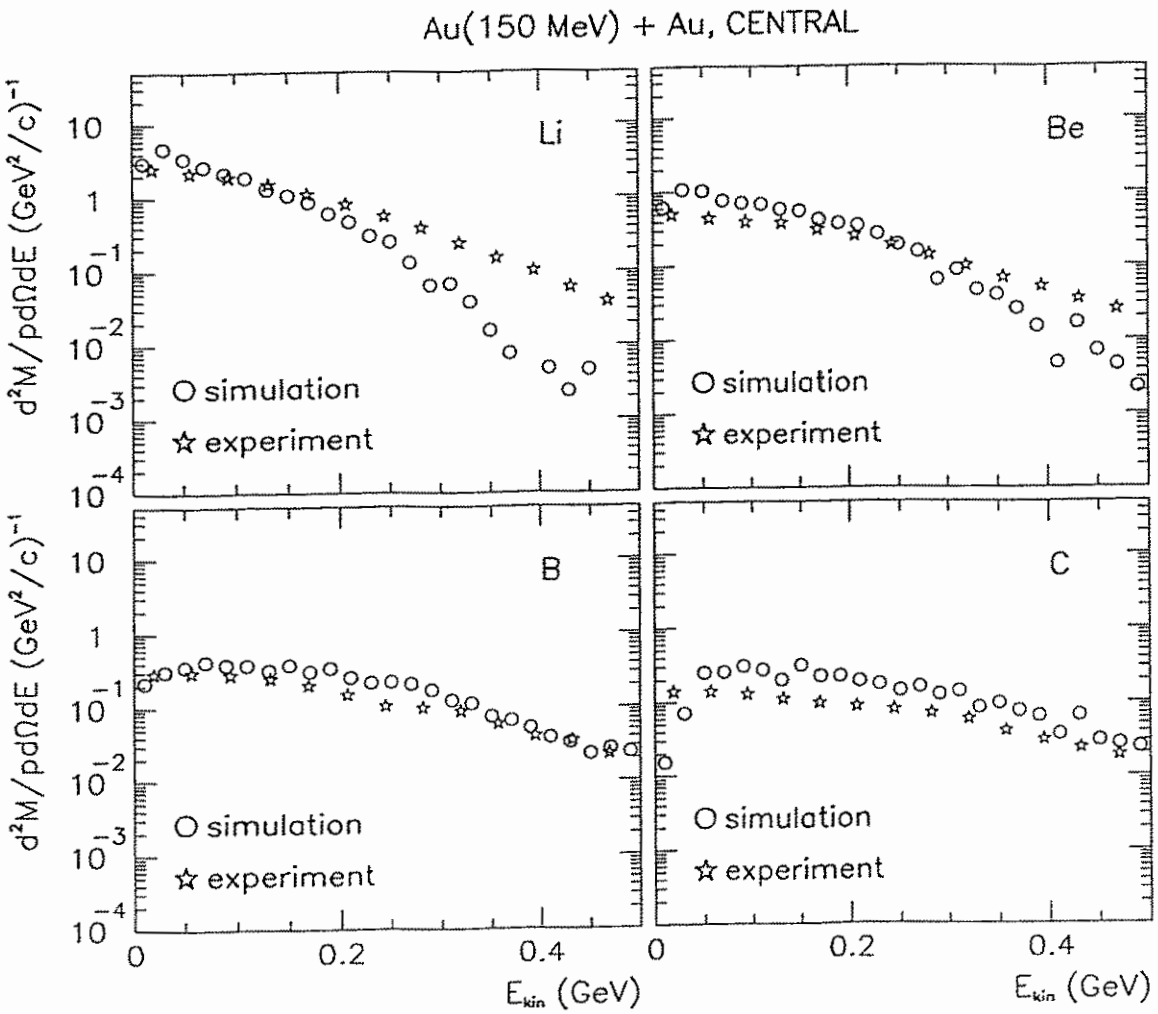

Fig. 10 One-particle kinetic energy spectra of lithium, berylium, boron and carbon isotopes for central gold on gold collisions at 150 A·MeV beam energy in comparison with experiment [42].

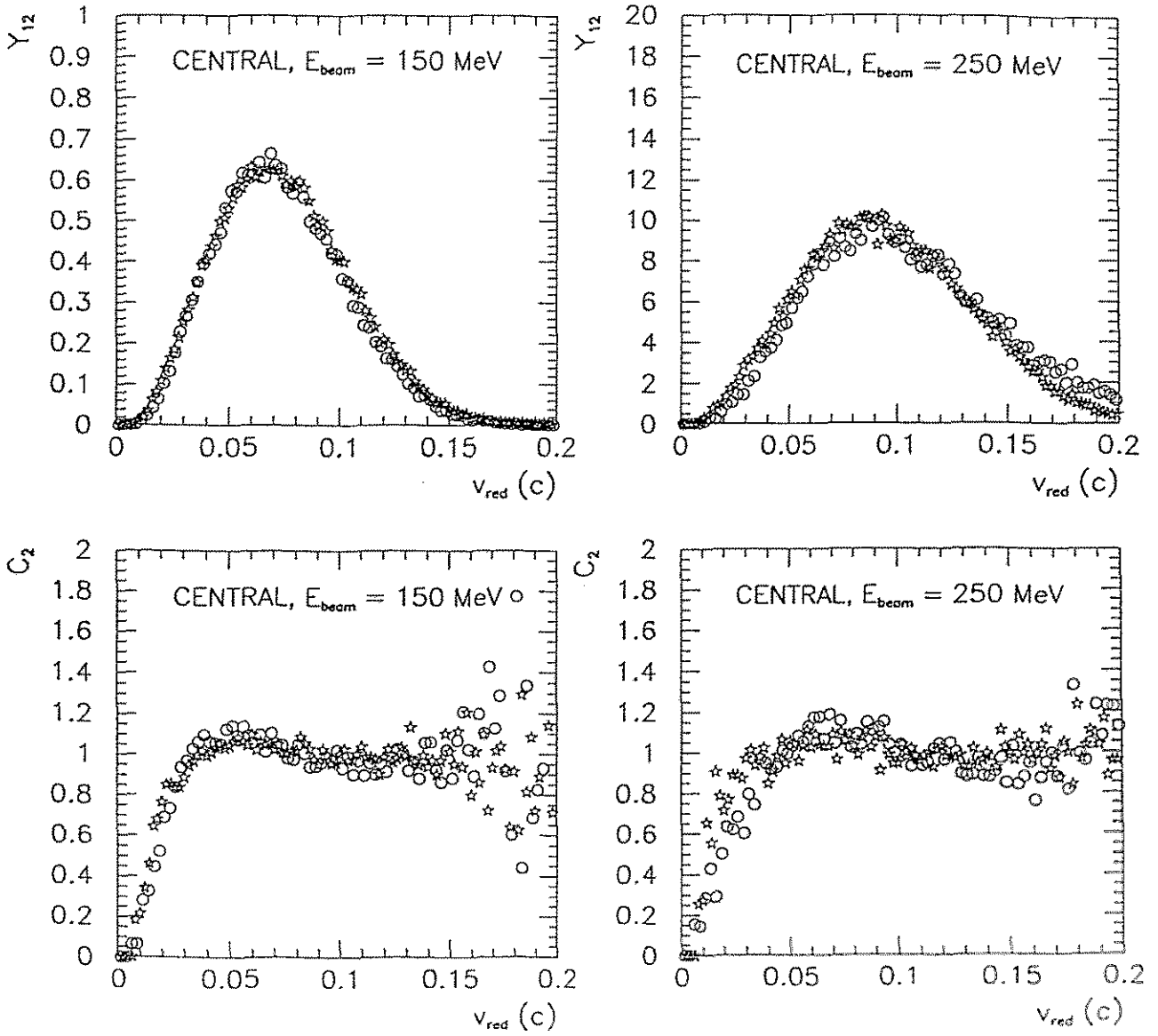

Fig. 11 Velocity distributions (upper panels) and correlation functions (lower panels) for central collisions. The stars belong to the experimental values [45] whereas the circles denote the calculated ones. The transverse flow energy has been reduced by a factor of 1/2 with respect to the values shown in fig. 5.

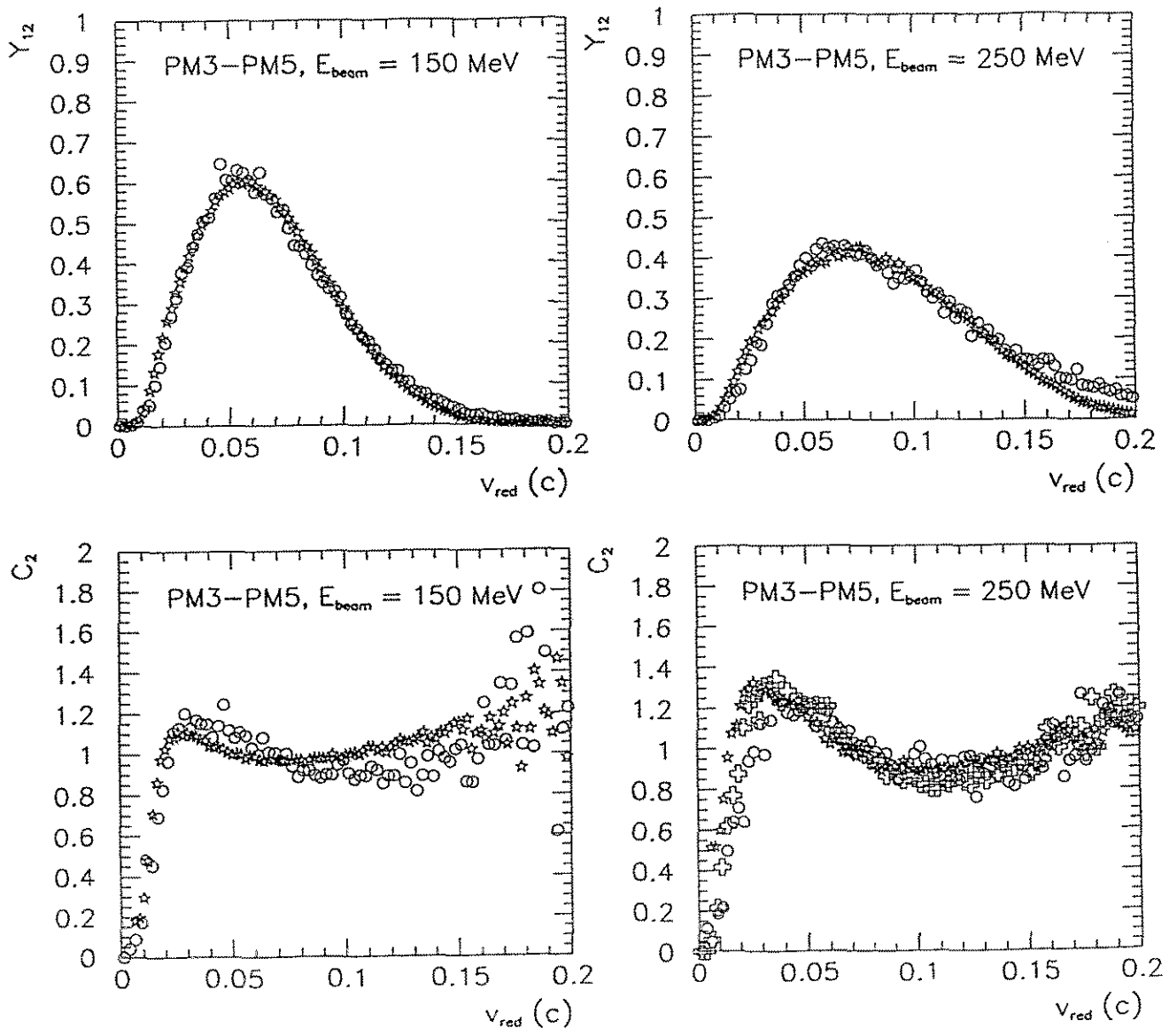

Fig. 12 Velocity distributions (upper panels) and correlation functions (lower panels) for semi-central collisions. The stars belong to the experimental values [45]. The calculation refers to both a reduction of transverse flow by a factor of 1/2 (circles) and a reduction of transverse flow by a factor of 1/4 (crosses).